



HAL
open science

Conductometric Sensor Based on Electropolymerized Pyrrole-Tailed Ionic Liquids for Acetone Detection

Hamdi Ben Halima, Anis Madaci, Emmanuel Contal, Abdelhamid Errachid-El-Salhi, Boris Lakard, Nicole Jaffrezic-Renault, Lydie Viau

► **To cite this version:**

Hamdi Ben Halima, Anis Madaci, Emmanuel Contal, Abdelhamid Errachid-El-Salhi, Boris Lakard, et al.. Conductometric Sensor Based on Electropolymerized Pyrrole-Tailed Ionic Liquids for Acetone Detection. ACS Applied Polymer Materials, 2024, 6 (8), pp.4718-4729. 10.1021/acsapm.4c00295 . hal-04552412

HAL Id: hal-04552412

<https://hal.science/hal-04552412>

Submitted on 19 Apr 2024

HAL is a multi-disciplinary open access archive for the deposit and dissemination of scientific research documents, whether they are published or not. The documents may come from teaching and research institutions in France or abroad, or from public or private research centers.

L'archive ouverte pluridisciplinaire **HAL**, est destinée au dépôt et à la diffusion de documents scientifiques de niveau recherche, publiés ou non, émanant des établissements d'enseignement et de recherche français ou étrangers, des laboratoires publics ou privés.

A Conductometric Sensor Based on Electropolymerized Pyrrole-Tailed Ionic Liquids for Acetone Detection

Hamdi Ben Halima¹, Anis Madaci², Emmanuel Contal¹, Abdelhamid Errachid², Boris Lakard¹, Nicole Jaffrezic-Renault^{2*}, Lydie Viau^{1*}

¹ Université de Franche-Comté, UMR CNRS 6213, 16 Route de Gray, Institut UTINAM, 25030 Besançon, France.

² Institute of Analytical Sciences (ISA) – UMR 5280, Claude Bernard Lyon 1 University (UCBL), 69100, Lyon, France.

* nicole.jaffrezic@univ-lyon1.fr ; lydie.viau@univ-fcomte.fr

ABSTRACT

The detection of acetone is of great significance for environmental safety and human health. In this work, a conductometric transducer was developed for the detection of acetone vapor. For this, interdigitated electrodes were functionalized by electropolymerization of a series of *N*-(1-methyl-3-octylimidazolium)pyrrole [PyC₈MIm]X monomers that contains different counter-anions X⁻, namely hexafluorophosphate (PF₆⁻), tetrafluoroborate (BF₄⁻) and bis(trifluoromethylsulfonyl)imide (TFSI⁻). The functionalized interdigitated electrodes were widely characterized. The analytical performances of the microsensors were determined in the presence of gaseous ethanol, acetone, toluene, chloroform, and methanol, collected from the headspace above aqueous solutions of known concentration. The gas-sensing responses of the films were measured at room temperature, through differential conductometric measurements conducted at 10 kHz. Among the different sensors, the one bearing BF₄⁻ anions presented the best analytical performance and was able to selectively detect acetone vapors. The response time (t_{Res}) of the sensor varied from 6 to 13s from lower to higher concentrations. The detection limit was 0.76 v/v % (7600 ppm) in the gas phase. The relative standard deviation for the same sensor was 6% for lower concentrations, and 2% for higher concentrations. The acetone sensor presented 2 times lower sensitivity for ethanol, and 4 times lower sensitivity for methanol. A detection of acetone in the headspace of a nail varnish remover sample led to an acetone content being in good agreement with the value given by the producer.

KEYWORDS

Polypyrrole, ionic liquids, electropolymerization, sensing, acetone

1. INTRODUCTION

Acetone, the simplest and smallest ketone is a colorless, volatile and flammable liquid that is widely used in cleansing purposes both in the chemical industry and research institutes due to its miscibility with water.¹ Besides its use as solvent, it is also widely utilized as reactant and extractant and is applied in the medical, pesticide and paint industries.² The common household use is in nail polish remover and as a paint thinner. Acetone is considered as the least toxic industrial solvent.³ However, high concentration vapor exposure should be avoided. Indeed, it has been demonstrated that exposure to acetone for a long time can cause several health problems such as headache and nausea. Hence, analyzing the acetone concentration in the environment is important for health and industrial safety. The analysis of acetone concentration in the breath has great potential for non-invasive diagnosis of the diabetic state. In healthy people, acetone concentration ranges from 0.2 to 0.9 ppm whereas in diabetic patients this acetone level ranges from 0.9 to 1.8 ppm.⁴ To date, huge efforts have been made towards the development of a simple and inexpensive sensor capable of detecting acetone gas at ppb level.

Sensing materials for conductimetric acetone sensors are usually composed of n-type semiconductors^{5, 6} such as ZnO,^{7, 8} TiO₂,⁹ SnO₂,¹⁰ and WO₃.¹¹ Conducting polymers such as polypyrrole (PPy) and polyaniline, that are easily synthesized and can operate at room temperature, have also been used as acetone sensing materials.^{12, 13} The influence of the deposition method on PPy-based acetone sensors properties (chemical oxidation casting, chemical vapor deposition, impregnated oxidation) has been studied by Do et al.¹⁴ They found that, in the presence of acetone, the sensors behave differently with acetone acting either as oxidant or reducing agent thus leading to an increase or a decrease of conductivity. The response (t_{Res}) and recovery times (t_{Rec}) of their sensors were in the range 0.5-18 min and 2-30 min, respectively. The group of Sirivat has studied different parameters that controlled the sensing properties of polypyrrole towards acetone. They prepared different polypyrrole films using various dopants and discussed their effect on the electrical response of PPy toward acetone vapor. They evidenced that the PPy structure with the most important proportion of polaron and bipolaron species presents the highest efficiency toward acetone vapor due to H-bond formation between the vapor molecules and the PPy chain and reduction of charge carrier species in the doped PPy sensor.¹⁵ This mechanism occurs when the solvent molecule presents a polar molecular function. Some polypyrrole films have also shown to be more efficient towards alcohol than acetone due to different chemical's polarity.^{16, 17} However, a

PPy film electrochemically deposited on a piezoelectric crystal, doped by Et_4NBF_4 presented higher selectivity toward acetone than ethanol with response time of about 60s.¹⁸ A portable gas analyzing system has also been developed using PPy to analyze diabetic patient's breath.¹⁹ Polypyrrole nanocomposites sensors containing Ag nanoparticles,²⁰ CdTe,²¹ or WO_3 ²² have also been developed for acetone detection. Recently, a PPy nanotube-based sensor with a detection limit of 500 ppb at 25°C toward acetone was reported.²³

On the other hand, Ionic Liquids (ILs) also present many interesting properties to be used in sensors design. They have negligible vapor pressure, wide electrochemical potential window, high thermal stability, and present high solubility for a broad range of gases.²⁴ The remarkable dissolution of the analytes allows to enhance the sensor's sensitivity while the non-covalent IL-analyte interactions permits the reversibility. One of the main key points is that the ILs' properties can be tuned by an appropriate choice of the cation/anion combination. The field of ILs-based gas sensors is mainly occupied by the development of amperometric sensors.^{25, 26} However, other sensors for vapor sensing have been developed. In 2002, Dai et al reported for the first time the use of ILs as sensing device for a quartz crystal microbalance device. Upon solubilization of the analytes, the viscosity of the IL changed resulting in a frequency shift of the quartz crystal. These sensors presented a fast response time of less than 2s and an excellent reversibility. The frequency shift was dependent to the nature of the IL (cation and anion) and of the nature of the vapors.²⁷ A similar sensor was developed specifically for acetone using [BMIm]BF₄ IL showing linear range from 7.5 to 705 ppm with fast response time.²⁸ A colorimetric sensor for acetone detection composed of TiO₂ particles coated with 1-H-3-methylimidazolium acetate IL was proposed by Nishan et al. The TiO₂ particles acted as photocatalyst while the IL induced electron in the conduction band of the particles. A colored eosin dye changed color after reaction with acetone in the presence of the TiO₂-coated particles.²⁹ For the development of IL-based gas and vapor sensors, their immobilization on a solid support is required. In this purpose, Poly(Ionic Liquids) (PILs) have also been used for sensing applications with the objective to combine the sensing ability of the IL with the mechanical processability of the polymer. Several examples of ions sensing, bio-sensing, gas, and solvent sensing have been reported.³⁰ For solvent sensing, different detection methods have been used such as color change, shape, and conductivity.³¹ PILs are known to behave as soft actuators and are thus prone to undergo molecular motion when submitted to an external stimulus.³² The response to acetone vapor of a porous polymer actuator was described by Yuan et al.³³ The actuation depends on the anion of the PIL and then on the solubility of the

solvent into the PIL and can also be coupled to the different vapor pressure of the solvent. Finally, PILs nanocomposites have been deposited on interdigitated electrodes to be used as a conductimetric solvent sensors.³⁴ To our knowledge, the electropolymerization method has never been used to elaborate solvent sensors using ionic liquid-like electroactive monomer. In this study, we prepared different sensors on gold interdigitated electrodes *via* the electrochemical polymerization of a pyrrole-functionalized imidazolium electroactive monomer bearing different anions (tetrafluoroborate, hexafluorophosphate, and bis(trifluoromethane)sulfonylimide). The analytical performance of the different sensors was tested against different solvent vapors (ethanol, acetone, toluene, chloroform, methanol, and water). The best candidate was then evaluated for the detection of acetone in a commercial nail varnish remover sample.

2. EXPERIMENTAL SECTION

2.1. Microconductometric chip

The microconductometric chip is presented in Figure 1. This chip is provided by Covarians company (Gif-sur-Yvette, France). It is fabricated by the printed circuit board technology.

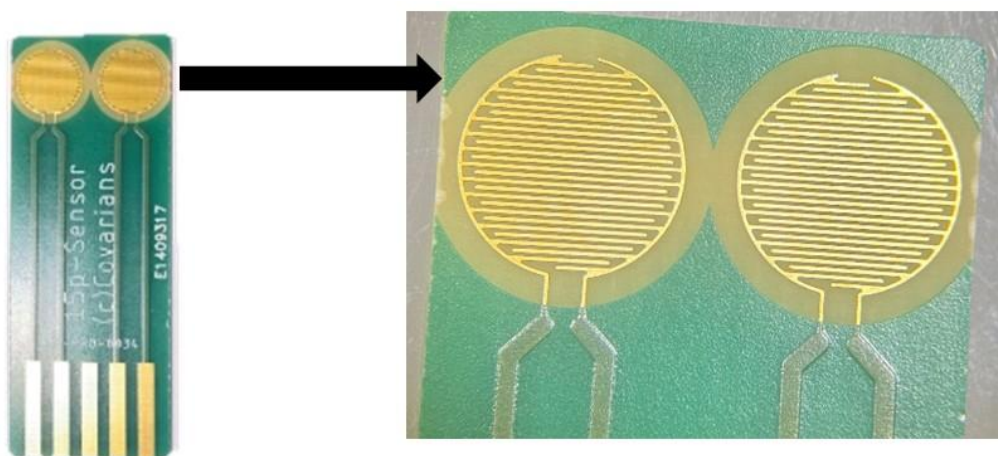
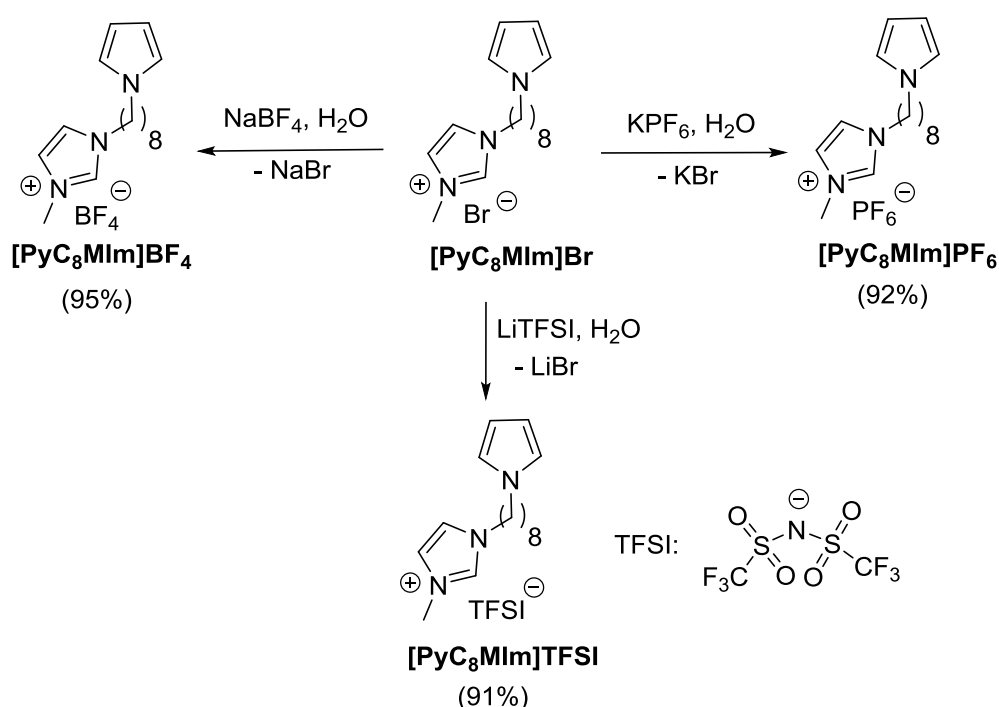


Fig. 1. Microconductometric chip: two pairs of interdigitated electrodes

The width of the interdigitated electrodes is 100 μm and the interelectrode distance is 100 μm . The electrodes in copper (42 μm thick) are deposited on a Printed Circuit Board (PCB) support, then covered by a layer of nickel (3 to 6 μm) and finally a layer of gold is deposited (50 to 120 nm).

2.2. Synthesis of the pyrrole-functionalized monomers

The synthesis route for the pyrrole-functionalized imidazolium monomers is featured in Scheme 1. The three monomers $[\text{PyC}_8\text{MIm}]\text{BF}_4$, $[\text{PyC}_8\text{MIm}]\text{PF}_6$ and $[\text{PyC}_8\text{MIm}]\text{TFSI}$ were obtained by anion metatheses of $[\text{PyC}_8\text{MIm}]\text{Br}$ ^{35, 36} with sodium tetrafluoroborate, potassium hexafluorophosphate and lithium bis(trifluoromethylsulfonyl)imide (see experimental details in ESI). The structure and the purity of the synthesized monomers were confirmed by ¹H, ¹³C, ¹⁹F, and ³¹P NMR analyses, ATR-IR spectroscopy, and mass spectrometry (Figures S1-S13).



Scheme 1. Synthesis of Pyrrole-functionalized imidazolium Ionic Liquids $[\text{PyC}_8\text{MIm}]\text{X}$ ($\text{X} = \text{BF}_4^-$, PF_6^- and TFSI⁻).

2.3 Electrochemical deposition of PPy films onto interdigitated gold electrodes

The microconductometric chip was treated under sonication in ethanol for 30 min and in acetone for 30 min and then was thoroughly rinsed with Milli-Q water, dried under a nitrogen flow. The conductometric measurements were carried out in a differential mode between a working sensor and a reference sensor. The working sensors were prepared by a two-step successive electropolymerization procedure (see below). This approach was necessary as attempts to electropolymerize $[\text{PyC}_8\text{MIm}]\text{X}$ monomers alone always led to poorly adhesive

films on the interdigitated electrodes. The reference sensor was covered by a single film of polypyrrole. By this way, the signal due to the PILs film will be directly measured.

Cyclic voltammetry (CV) experiments were performed with a SP-200 potentiostat from Biologic controlled with a PC computer via EC-Lab V11.43 software interface. Electrochemical experiments were performed using a three-electrode setup with interdigitated gold electrode as working electrode, a Saturated Calomel Electrode (SCE) reference electrode and a platinum sheet as counter-electrode. The first layer of polypyrrole was obtained via CV using a 0.1 M acetonitrile solution of the pyrrole monomer containing 0.1 M LiClO₄ in the potential range from -0.6 to 1.8V/SCE with a scan rate of 100 mV/s, along 7 cycles.

As shown in Figure 2A, the cyclic voltammogram (CV) obtained for the pyrrole monomer presents a wide anodic peak at 0.75V/SCE encompassing the oxidation of pyrrole monomers and the oxidation of polypyrrole, and a cathodic peak at 0 V/SCE corresponding to the reduction of polypyrrole. The current increases after each cycle with confirmed that our deposited polymer (PPy) is conductive and that the amount of polymer on the electrode surface increases upon cycling. A black thin solid film is observed onto the interdigitated electrode confirming that the electropolymerization has been successfully performed.

For the working sensors, on top of the polypyrrole film, we performed the electropolymerization of the pyrrole-functionalized Ionic Liquids [PyC₈MIm]X (X= BF₄⁻, PF₆⁻, TFSI⁻) (0.1M in CH₃CN) + NaBF₄/KPF₆/LiTFSI (0.1 M) using cyclic voltammetry in the range -0.6 to 1.8 V/SCE at a scan rate of 100 mV/s, along 4 cycles. After polymerization, the films are named accordingly: PPy, PPy-PPyBF₄, PPy-PPyPF₆ and PPy-PPyTFSI.

Figs 2B-D show that the shape of the CVs obtained were very similar whatever the anions with the presence of oxidation and reduction peaks of polypyrrole. With X = TFSI, the CV presents a slightly lower current intensity that might be due to less charging-discharging redox process in the presence of the large TFSI⁻ anion showing average mobility.³⁷ In all cases, the increase of the current intensity confirms the formation of conductive PPy-PPyX films on top of the polypyrrole one.

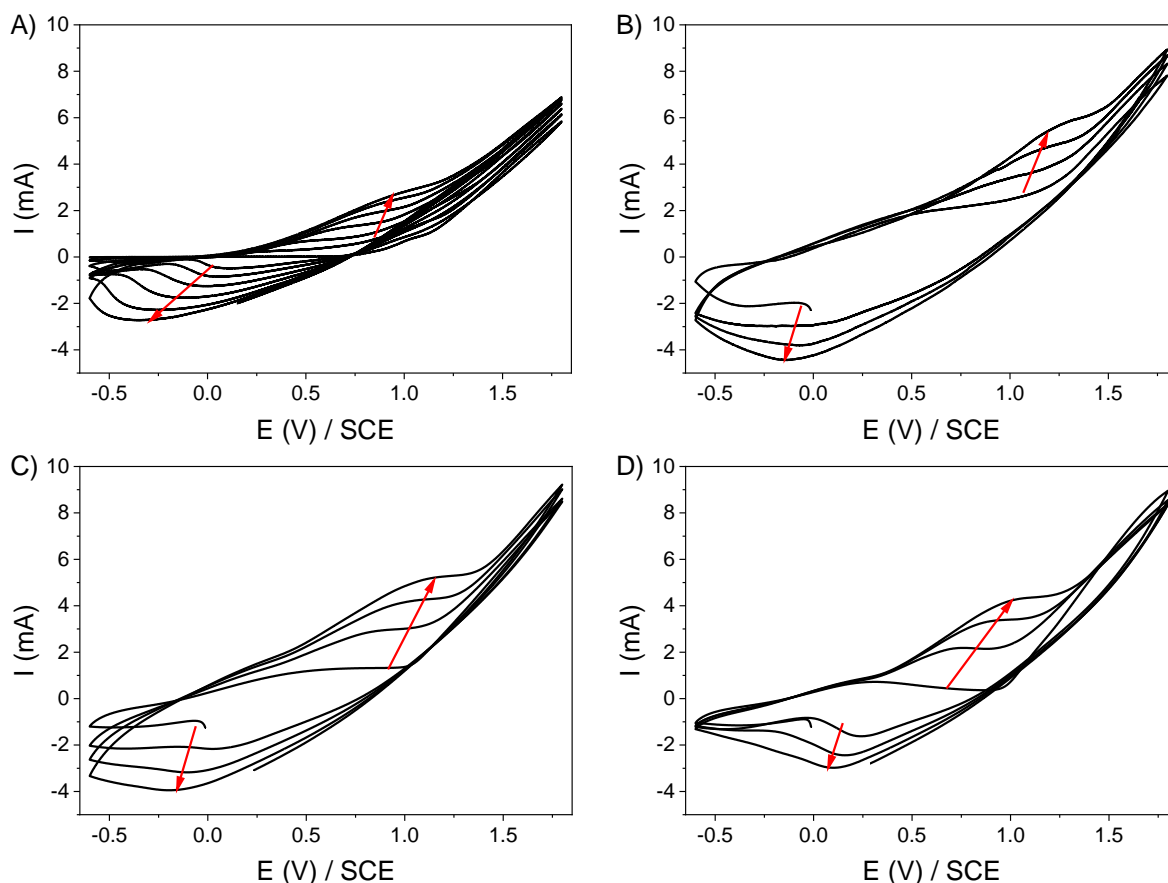


Fig. 2. Comparison between cyclic voltammograms during the electropolymerization of (A) pyrrole and the pyrrole-functionalized Ionic Liquids [PyC₈MIm]X (B) X = BF₄⁻, (C) X = PF₆⁻, (D) X = TFSI on top of the PPy film.

2.4 Micro conductometric measurements

Conductometric detection was achieved by applying to each pair of IDEs (sensors) a small-amplitude sinusoidal voltage (10 mV peak-to-peak at 0 V) at a 10 kHz frequency generated by a “VigiZMeter” conductometer manufactured by the company “Covarians”, and the responses of the gas sensor were recorded at room temperature (23 ± 1 °C), as a function of time. The differential output signal was recorded between the working and the reference pairs of IDEs.

Conductometric measurements were made after introducing the working sensor and the reference sensor in the headspace (volume of the gas exposure chamber: 15 cm³) over the liquid phase (volume: 10 cm³) in a cylindrical container for one minute and then withdrawing it (Figure 3). The differential measurement of conductance (ΔG) was recorded versus time. The response time (t_{Res}) describes the time necessary to reach 90% of the total change of conductance and the recovery time (t_{Rec}) characterizes the time necessary to recover 10% of the total change in conductance.

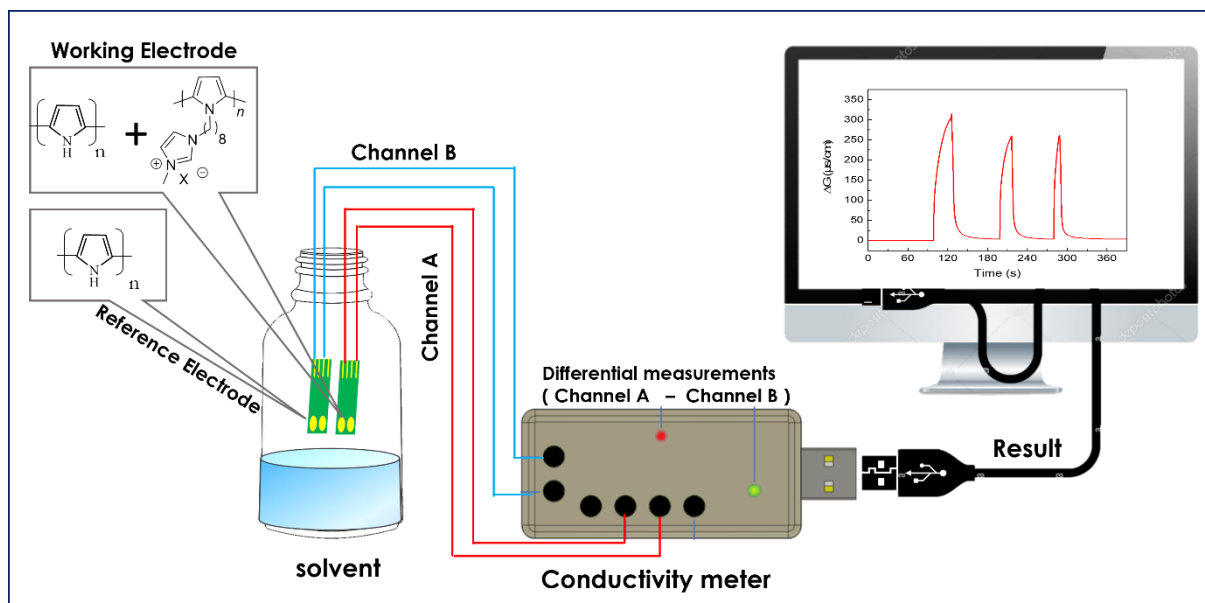


Fig. 3. Diagram of the experimental setup: measurement in the headspace above the liquid phase.

2.5 Preparation of VOC samples

Gaseous ethanol, acetone, toluene, chloroform, and methanol samples were collected from the headspace above aqueous solutions of known concentration (5%-100%). The concentration of samples in the gas phase above aqueous solutions depends on Henry's law constants of the given analyte in water and was calculated from Henry's law following the equation given by Sander (25°C)³⁸ (equation 1):

$$k_H^0 = \frac{c_a}{p_g} \quad (1)$$

where k_H^0 (in M/atm) is the Henry's law constant for standard conditions; c_a is the aqueous concentration of the analyte in M, and p_g (atm) is the partial pressure of the analyte in the gas phase.

For ethanol, acetone, and methanol, k_H^0 values of $1.9 \cdot 10^2$ M/atm, $0.24 \cdot 10^2$ M/atm, , $2.2 \cdot 10^2$ M/atm , were used, respectively.³⁹ In Tables S1, S2, and S3, the used equilibrium gas-phase concentrations above aqueous ethanol, methanol, and acetone solutions are specified.

2.6 Characterization techniques

Electrochemical Impedance Spectroscopy (EIS) measurements were performed using an electrochemical cell consisting of three electrodes. The reference electrode was a saturated calomel electrode, the auxiliary electrode was a platinum sheet and the interdigitated gold electrodes modified with the polymer film were used as working electrode. EIS measurements were carried out in the presence of the redox probe $[\text{Fe}(\text{CN})_6]^{3-}/[\text{Fe}(\text{CN})_6]^{4-}$ at 5 mM in a phosphate buffer solution (PBS, pH 7.4), with a frequency ranged from 100 kHz to 1 Hz, two frequency points per frequency decade, and using a modulation voltage of 10 mV (E_{ac}). During the measurements, the potential was kept at 0.2 V/SCE (E_{dc}). Data fitting on EIS spectra was performed with Randomize (5000 iterations) + Simplex method (fit stopped on 5000 iterations) and the following equivalent circuit model $[R_s + Q_2 / R_{ct}]$ where R_s is the electrolyte solution's resistance ($[\text{Fe}(\text{CN})_6]^{3-/4-}$), the parallel elements are Q_2 (the coefficient of the constant phase element), and R_{ct} (the charge transfer resistance).

Mechanical Profilometry. The thickness (T) and arithmetic roughness (R_a) of PPy or PPy-PPyX films were measured by profilometry using a stylus (2.5 μm)-based mechanical probe profiler Alpha-Step IQ from KLA Tencor. Both thickness and roughness were measured on a scan length of 1000 μm at a scan speed of 25 $\mu\text{m}\cdot\text{s}^{-1}$. Reported thickness and roughness are the means of at least 5 measurements done at different places of the samples.

Water Contact Angles (WCA) of the modified and unmodified Au substrates were measured by using a GBX Scientific Instruments contact angle analyzer (Digidrop Contact Angle Meter used with Windrop software) with 2 μL water drops with a dosing rate of 0.58 $\mu\text{L}\cdot\text{s}^{-1}$. The drop was formed on the tip of a syringe needle and placed onto the sample surface by raising the sample until contact was made. Contact angles were determined by drawing the tangent close to the edge of the droplet. For each sample at least 5 measurements were performed.

Infrared Spectra were recorded on a Bruker vertex70 FTIR spectrometer equipped with a DGTS detector using a Platinum ATR accessory equipped with a diamond crystal. For each sample, 128 scans were recorded with a 4 cm^{-1} resolution.

Scanning Electron Microscopy (SEM). The surface morphology of PPy and PPy-PPyX films was obtained, without metallization treatment, using a high-resolution scanning electron microscope MIRAN3 TESCAN with an electron beam energy of 7 keV.

X-Ray Photoelectron Spectroscopy. Chemical surface analyses of the samples were studied on a Versaprobe 5000 spectrometer (ULVAC-PHI, Inc.) equipped with a monochromatized and a focalized Al K α X-ray source (1486.6 eV). For each sample, survey spectra, as well as high-resolution core-level region were acquired over a spot size of 200 μm . To record the survey spectra and high-resolution regions, pass energies of 187.5 eV and 58.7 eV were used, respectively. Data processing was done using Casa XPS software⁴⁰ and energy calibration was done on C1s CC/CH bonds at 284.6 eV. The quantification was obtained from the measurement of the corresponding peak area and the use of relative sensitivity factors (RSF), specific of the spectrometer and provided by the manufacturer.

3. RESULTS AND DISCUSSION

3.1 Characterization of the PPy films using EIS

EIS characterization was used to evidence different charge transfer process occurring at the electrode-electrolyte interfaces. Fig. 4 presents the impedance data as Nyquist plots. The charge transfer resistance (R_{ct}) values on the electrode surface were determined after fitting and all calculated values of the equivalent circuit are presented in Table 1. As expected, the values of the electrolyte resistance (R_s) are very similar, close to 40 Ω and the Q_2 values that correspond to a constant phase element associated with the electrical double layer gold/PPy film/electrolyte solution increased after functionalization of the gold substrates with the conductive polypyrrole films. The R_{ct} value decreases from 339 Ω for neat gold electrode to 240 Ω after electropolymerization of pyrrole. Such a decrease is due to the fact that polypyrrole is conductive and the electrons are then easily conducted to the interface. This result is in accordance with those obtained by cyclic voltammetry (*see vide supra*). In line also with the results from CV experiments, a decrease of R_{ct} values is observed after following polymerization with [PyC₈MIm]X monomers due to the formation of more conductive films. The R_{ct} values are very close for PPy-PPyPF₆ and PPy-PPyTFSI samples, 32 and 34 Ω , respectively. However, the PPy-PPyBF₄ sensor presents a higher R_{ct} value of 121 Ω . These differences of charge transfer resistance might be explained by different morphology features (*see vide infra*).

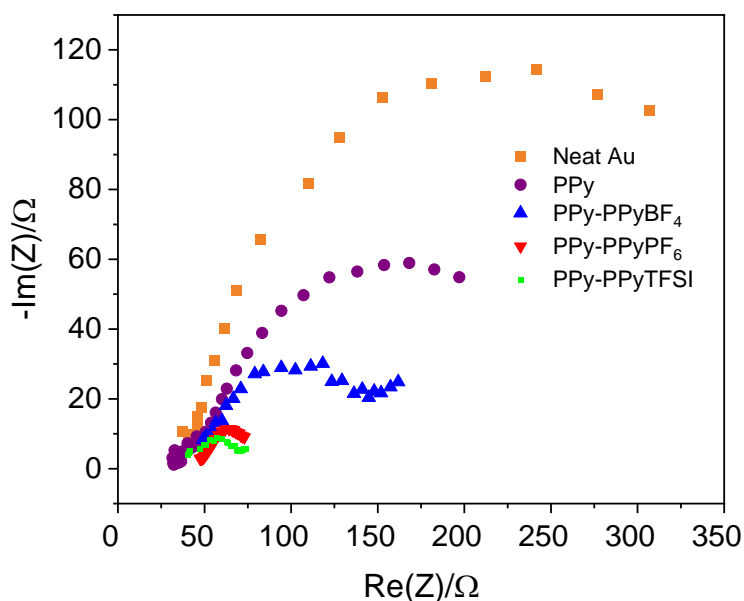


Fig. 4. Nyquist plot obtained after the different steps of polymerization. Neat Au, Neat Au + PPy), Neat Au + PPy-PPyBF₄, Neat Au + PPy-PPyPF₆, Neat Au + PPy-PPyTFSI in 5 mM [Fe(CN)₆]^{3-/4}, initial potential E = 0.2 V/SCE. Highest Freq = 100 kHz, Lowest Freq = 1 Hz.

Table 1. Results of fitting the Nyquist plots using the model [R_s + Q₂/ R_{ct}] of the EIS measurements for the different steps of functionalization; χ^2 is the error on the fit.

Samples	R _s (Ω)	Q ₂ (F.s ^(a-1))	R _{ct} (Ω)	χ^2
Neat Au	40.47	7.485×10 ⁻⁶ (a=0.756)	339	8.484×10 ⁻³
PPy	41.58	3.079×10 ⁻³ (a=0.576)	240	5.110×10 ⁻³
PPy-PPyBF ₄	40.72	0.263×10 ⁻³ (a=0.576)	121	3.698×10 ⁻³
PPy-PPyPF ₆	47.8	5.705×10 ⁻³ (a=0.568)	32	8.470×10 ⁻³
PPy-PPyTFSI	39.66	0.386×10 ⁻³ (a=0.572)	34	1.603×10 ⁻³

3.2 Physico-Chemical Characterization of the films

3.2.1 Infrared spectroscopy (FT-IR) analysis

FT-IR measurements were also used to confirm the formation of polypyrrole and the incorporation of the [PyC₈MIm]X moiety. As shown in Fig. 5A, the FT-IR spectrum of PPy

presents bands characteristic of polypyrrole.^{41, 42} The band at 1548 cm^{-1} is attributed to ring stretching vibration of C-C and C=C bonds, those at 1296 and 1036 cm^{-1} are due to the =C-H in-plane vibrations, the band at 1172 cm^{-1} is due to the C-N stretching vibrations, the bands at 905 and 965 cm^{-1} due to C-H (-HC = CH-) vibrations, and the bands from 667 - 781 cm^{-1} corresponds to C-H_{Aromatic} vibrations. The IR spectra of PPy-PPyBF₄, PPy-PPyPF₆ and PPy-PPyTFSI present similar bands at 2854 - 2924 cm^{-1} that correspond to $\nu_{\text{C-H}}$ alkyl groups and bands at 3110 - 3155 cm^{-1} attributable to $\nu_{\text{C-H}}$ imidazolium ring vibrations.⁴³ The bands characteristic to polypyrrole are less intense. The FT-IR spectrum of PPy-PPyBF₄ (Fig. 5B) shows an intense band at 1051 cm^{-1} attributed to B-F stretching vibration that confirms the presence of BF₄⁻ anions,⁴⁴ the one of PPy-PPyPF₆ (Fig. 5C) presents a very strong band at 936 cm^{-1} (ν_{as} P-F)⁴⁵ and finally for PPy-PPyTFSI (Fig. 5D) new characteristic bands of TFSI at 1350 and 1132 cm^{-1} (ν_{as} and ν_{s} SO₂), at 1180 cm^{-1} (ν_{as} CF₃), and at 615 cm^{-1} (δ_{a} SO₂)⁴⁶ are present.

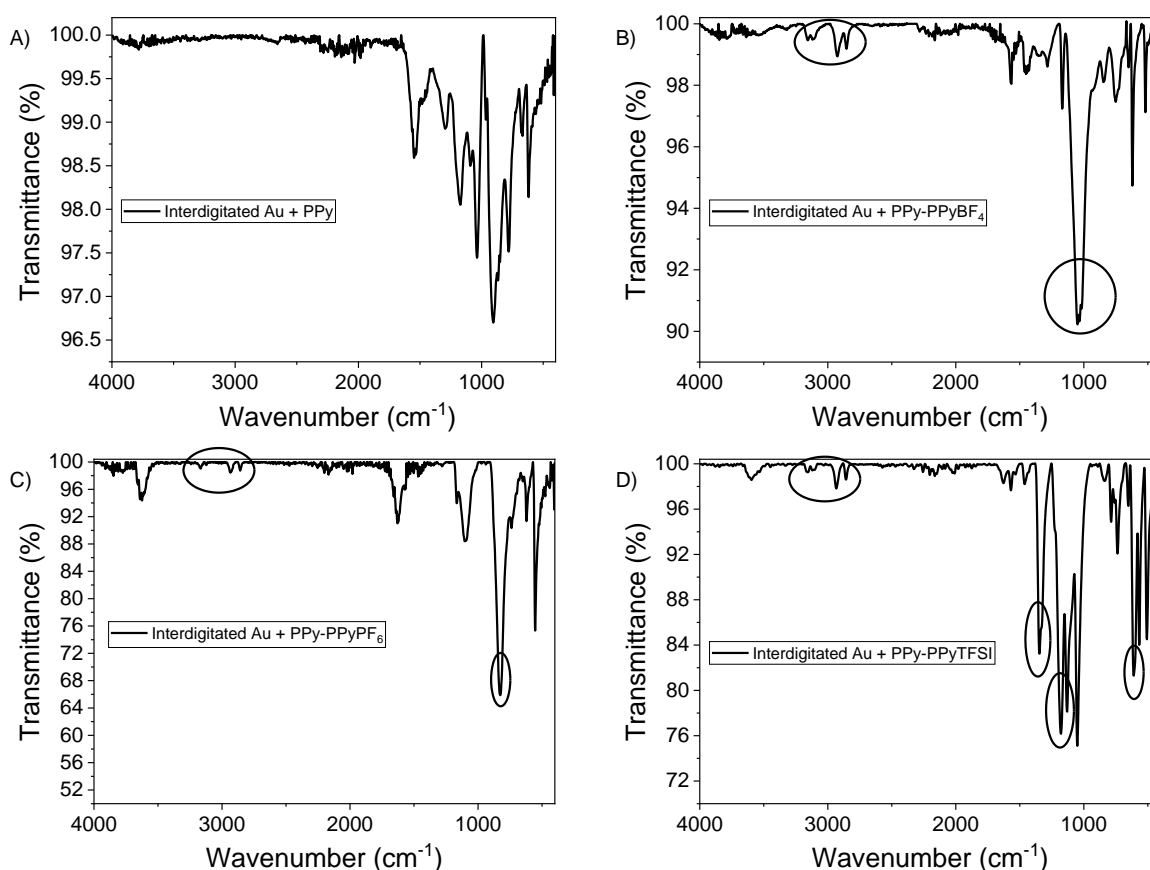
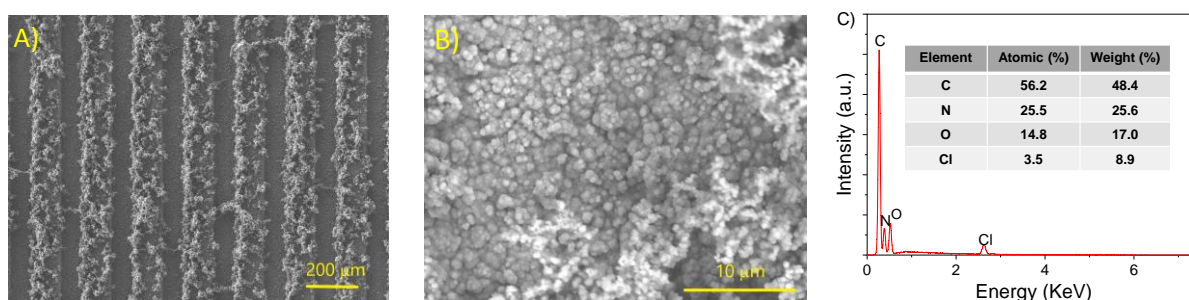


Fig. 5. FT-IR spectra of A) PPy; B) PPy-PyBF₄, C) PPy-PyPF₆, and D) PPy-PyTFSI onto the interdigitated gold electrodes.

3.2.2 Morphological features

Scanning electron microscopy (SEM) was used to determine the surface morphology of the polypyrrole films onto the interdigitated gold electrode. Fig. 6A-B show that the whole surface of the interdigitated gold microelectrodes is coated by a homogeneous film composed of small aggregates of polypyrrole nodules of few nanometers. Following the electropolymerization of [PyC₈MIm]BF₄ (Fig. 6E) onto the gold electrode previously coated with PPy the obtained film is more compact, homogenous, and of overall uniform surface morphology when compared to the PPy film. The PPy-PPyBF₄ electrode is composed of big PPy aggregates of 10 μm of diameter. The structure of the PPy-PPyPF₆ (Fig. 6G-H) and PPy-PPyTFSI (Fig. 6J-K) electrodes look rather similar with PPy aggregates of about 1 μm of diameter.

Each of the films obtained on interdigitated electrodes was analyzed by Energy-Dispersive X-Ray spectroscopy (EDX). Results are shown in Fig. 6. C, F, I, L. For PPy, clear signals characteristic of carbon, oxygen, nitrogen, and chlorine are observed. Carbon and nitrogen elements are the main components of polypyrrole while the presence of chlorine and oxygen confirms the doping of the polypyrrole scaffold with perchlorate anions. Additionally, the EDX spectra of PPy-PPyBF₄, PPy-PPyPF₆ and PPy-PPyTFSI present fluoride, an element present in the three different anions. The atomic percentages of Cl and O have also decreased showing that the surface is mainly composed of polypyrrole films bearing BF₄⁻, PF₆⁻ and TFSI anions. The EDX spectrum of PPy-PPyPF₆ presents also additional phosphorous element and the one of PPy-PPyTFSI presents the sulfur peak.



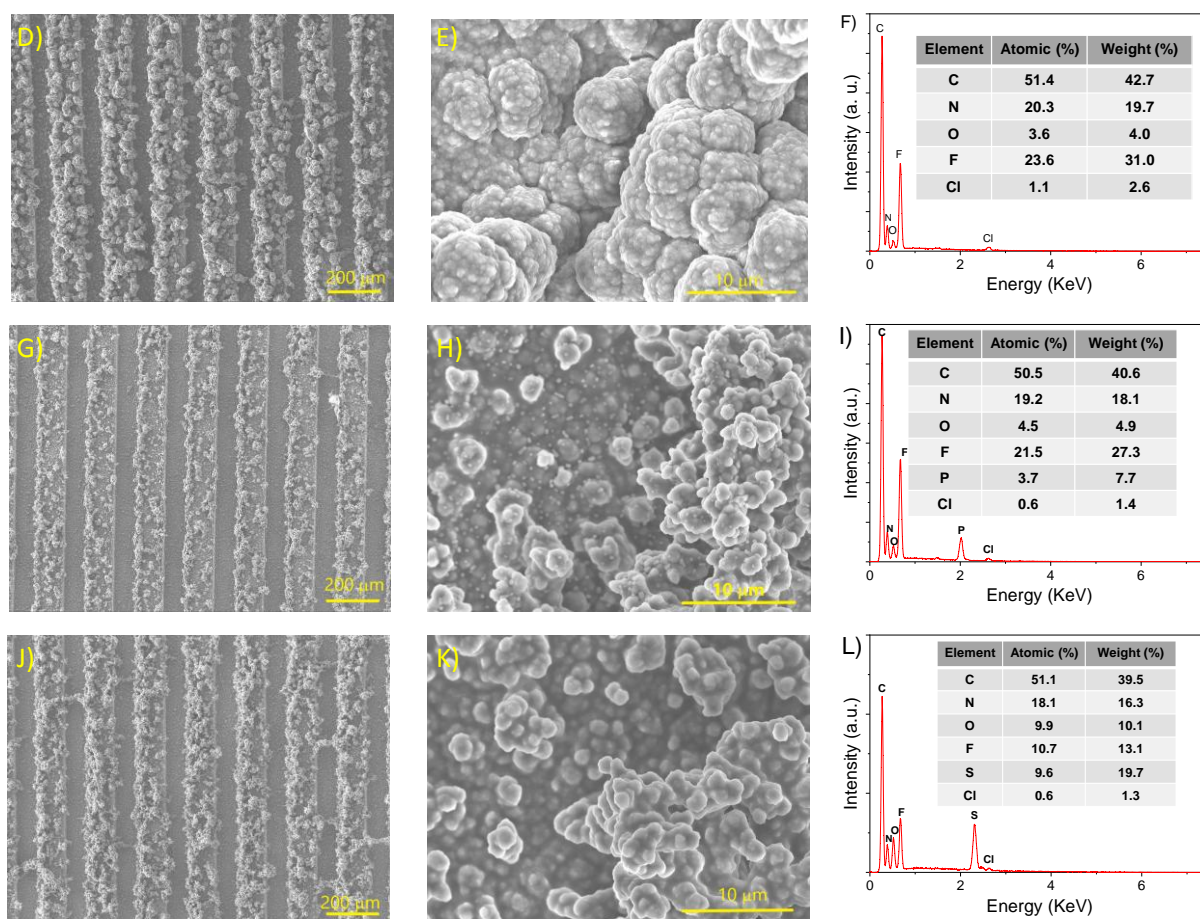


Fig. 6. SEM images of A, B) PPy D), E) PPy-PPyBF₄, G, H) PPy-PPyPF₆, J, K) PPy-PPyTFSI onto the interdigitated gold electrodes with corresponding EDX spectra.

The thicknesses of the electrodeposited films were measured by profilometry (Table 2). The thickness of the PPy film is $7.1 \pm 1.2 \mu\text{m}$ (with a roughness of $1.7 \pm 0.5 \mu\text{m}$), while the thicknesses of the PPy/pyrrole-functionalized Ionic Liquid films are $28.8 \pm 2.3 \mu\text{m}$ with a roughness of $2.4 \pm 0.7 \mu\text{m}$ for PPy-PPyBF₄, $27.3 \pm 3.7 \mu\text{m}$ with a roughness of $2.1 \pm 0.8 \mu\text{m}$ for PPy-PPyPF₆, and $24.2 \pm 1.7 \mu\text{m}$ with a roughness of $2.3 \pm 0.9 \mu\text{m}$ for PPy-PPyTFSI.

Table 2. Thickness (T) and average roughness (R_a) of the different electrodeposited films.

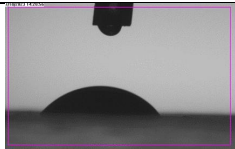
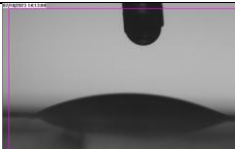
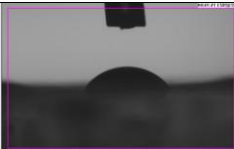
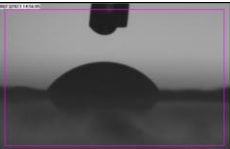
	PPy	PPy-PPyBF ₄	PPy-PPyPF ₆	PPy-PPyTFSI
T (μm)	$7.1 \pm 1.2 \mu\text{m}$	$28.8 \pm 2.3 \mu\text{m}$	$27.3 \pm 3.7 \mu\text{m}$	$24.2 \pm 1.7 \mu\text{m}$
Ra (μm)	$1.7 \pm 0.5 \mu\text{m}$	$2.4 \pm 0.7 \mu\text{m}$	$2.1 \pm 0.8 \mu\text{m}$	$2.3 \pm 0.9 \mu\text{m}$

3.2.3 Water Contact Angle

The efficiency of the deposition of different imidazolium-polypyrrole films onto the interdigitated electrodes was further assessed by water contact angle measurements (Table 3).

For PPy, a water contact angle of $49\pm 1^\circ$ was found. Following electropolymerization with [PyC₈MIm]X monomers, the water contact angle of PPy-PPyBF₄ fell to $24\pm 1^\circ$ due to the hydrophilic characteristic of the BF₄⁻ anions. For PPy-PPyPF₆ and PPy-PPyTFSI the water contact angles values ($50\pm 1^\circ$ and $55\pm 1^\circ$) are much larger than for PPy-PPyBF₄. This is in accordance with the fact that PF₆⁻ and TFSI⁻ anions are hydrophobic with TFSI⁻ being the most hydrophobic one.

Table 3. WCA results obtained on different sensors.

Samples	PPy	PPy-PPyBF ₄	PPy-PPyPF ₆	PPy-PPyTFSI
WCA (°)				
	49±1	24±2	50±1	55±1

3.2.4 XPS Analysis

In accordance with EDX analysis, the XPS survey spectrum of PPy revealed the presence of C1s, N1s, O1s, and Cl2p components as can be seen in Table 4. In addition to these peaks, PPy-PPyBF₄ shows signals at 685.6 eV and 193.6 eV with a 4:1 ratio attributable to F1s and B1s components stemming from the incorporation of BF₄⁻ anions. PPy-PPyPF₆ presents also additional peaks at 631.6 eV (F1s) and 136.6 eV (P2p) with a $\approx 6:1$ ratio coming from the incorporation of PF₆⁻ anions, while for PPy-PPyTFSI peaks at 686.2 and 166.6 eV are attributable, respectively, to F1s and S2p components of the TFSI⁻ anions (ratio 3:1).

Table 4. XPS data (binding energy (BE), and atomic percent) for PPy, PPy-PPyBF₄, PPy-PPyPF₆ and PPy-PPyTFSI.

Components	PPy		PPy-PPyBF ₄		PPy-PPyPF ₆		PPy-PPyTFSI	
	Peak BE (eV)	Atomic %	Peak BE (eV)	Atomic %	Peak BE (eV)	Atomic %	Peak BE (eV)	Atomic %
C1s	284.6	64.8	284.6	64.1	284.6	57.2	284.6	48.8
N1s	399.7	15.1	401.6	11.7	401.6	8.9	401.6	10.8
O1s	532.7	17.3	532.6	4.4	531.6	6.1	531.6	18.1
Cl2p	208.7	2.8	207.6	0.5	-	-	-	-

F1s	-	-	685.6	15.5	631.6	24.1	688.6	17.2
B1s	-	-	193.6	3.8	-	-	-	-
P2p	-	-	-	-	136.6	3.7	-	-
S2p	-	-	-	-	-	-	168.6	5.1

The high-resolution XPS spectra of the N1s core level peaks of PPy-PPyBF₄, PPy-PPyPF₆ and PPy-PPyTFSI shown in Fig. 7 were fitted with two components, one at *ca* 400.0 eV and one at *ca*. 401.8 eV (Table 5). The N1s spectra of polypyrrole is also known to contain two components at the same binding energy. The one at 400.0 eV corresponds to the amine like structure (-NH-) while the one at 401.8 eV corresponds to N-H⁺ and =N-H⁺ structures.⁴² The ratios' intensities between the components at 401.8 eV and 400.0 eV is equal to 0.2 for polypyrrole. The only difference between PPy and the imidazolium functionalized films stands from the ratio of these two peaks *i.e.* 1.9 for PPy-PPyBF₄, 3.3 for PPy-PPyPF₆ and 0.4 for PPy-PPyTFSI. The increase of the ratio intensity in the case of PPy-PPyBF₄ and PPy-PPyPF₆ is due to the presence of the imidazolium cation that presents a N1s peak at *ca* 401.5 eV^{47, 48}. For PPy-PPyTFSI, the ratio is close to the one of PPy as the increase of the component at 401.5 eV due to the incorporation of the imidazolium function is counter-balanced by the presence of TFSI anions that presents a N1s peak at 399.3 eV.⁴⁹

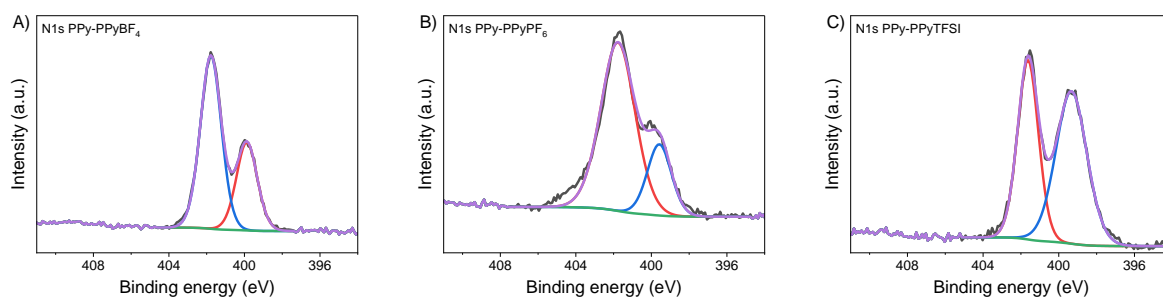


Fig. 7. High resolution N1s XPS spectra of A) PPy-PPyBF₄, B) PPy-PPyPF₆, and C) PPy-PPyTFSI.

Table 5. Assignments of the peaks present in the XPS N1s spectra (binding energy (BE), and atomic percent of electrodeposited films.

Sample	Peak BE (eV)	Atomic %	Assignment
PPy ⁴²	400.0	82.8	N-H
	401.8	17.2	N=H ⁺ and N-H ⁺

PPy-PPyBF₄	399.9	33.8	N-H
	401.8	66.2	N=H ⁺ , N-H ⁺ , N _{cation}
PPy-PPyPF₆	399.6	23.2	N-H
	401.8	76.8	N=H ⁺ , N-H ⁺ , N _{cation}
PPy-PPyTFSI	399.3	55.9	N-H, N(TFSI)
	401.6	44.1	N=H ⁺ , N-H ⁺ , N _{cation}

3.5 Analytical performance of the microconductometric sensors

Fig. 8 shows the comparison of the response of PPy-PPyBF₄, PPy-PPyPF₆ and PPy-PPyTFSI at the atmosphere of ethanol, acetone, toluene, chloroform, methanol, and water, respectively. As can be seen in Fig. 8, the PPy-PPyBF₄ sensor has a higher response towards acetone than the other solvent. Contrarily, the other sensors with PF₆⁻ and TFSI⁻ anions do not respond to acetone and to any other solvent. Only some response towards water was registered but to a lesser extent. Different phenomena can occur in the sensing mechanism and one possible explanation for the differences observed between the different anions may come from different solubility of a specific vapor in an IL. The difference in hydrophilicity plays an important role in determining the affinity of an IL toward a chemical vapor. Here, acetone is more hydrophobic than ethanol or methanol and should thus interact with the more hydrophobic IL i.e PPy-PPyTFSI. This is clearly the opposite trend that is observed, the more hydrophilic IL PPy-PPyBF₄ interacts more strongly with acetone. To explain the highest selectivity of the films bearing BF₄⁻ anions one may also invoke difference in morphology. However, SEM images have evidenced that PPy-PPyBF₄ is composed of large aggregates, much larger than in the PPy-PPyPF₆ and PPy-PPyTFSI films. It is known that PPy particles with smaller size are better gas sensing materials.⁵⁰ Thus, the difference in morphology observed in our case is not responsible for the different selectivity among the anions. Imidazolium-based ILs are known to interact with solvent molecules (acetonitrile, acetone..) *via* hydrogen bonding between the protons of the imidazolium ring and the hydrogen acceptor atoms present in the solvent.⁵¹ Simulation studies have evidenced that hydrogen bonding between imidazolium cations and different anions are stronger with TFSI⁻ anions than with BF₄⁻ ones and other studies have demonstrated higher hydrogen-bond strengths to the 1-n-butyl-3-methylimidazolium ion for PF₆⁻ compared to BF₄⁻ anions.⁵² Thus, BF₄⁻ anions are freer to interact with molecular solvent. At the same time, the higher selectivity for acetone than ethanol or methanol might thus be due to the preferential formation of hydrogen bonds

between the H atoms on the imidazolium cation and the oxygen of the carbonyl group of acetone^{53, 54} due to the higher polarity of acetone molecule (dipole moment of acetone 2.88 D dipole moment of methanol or of ethanol ≈ 1.9 D).

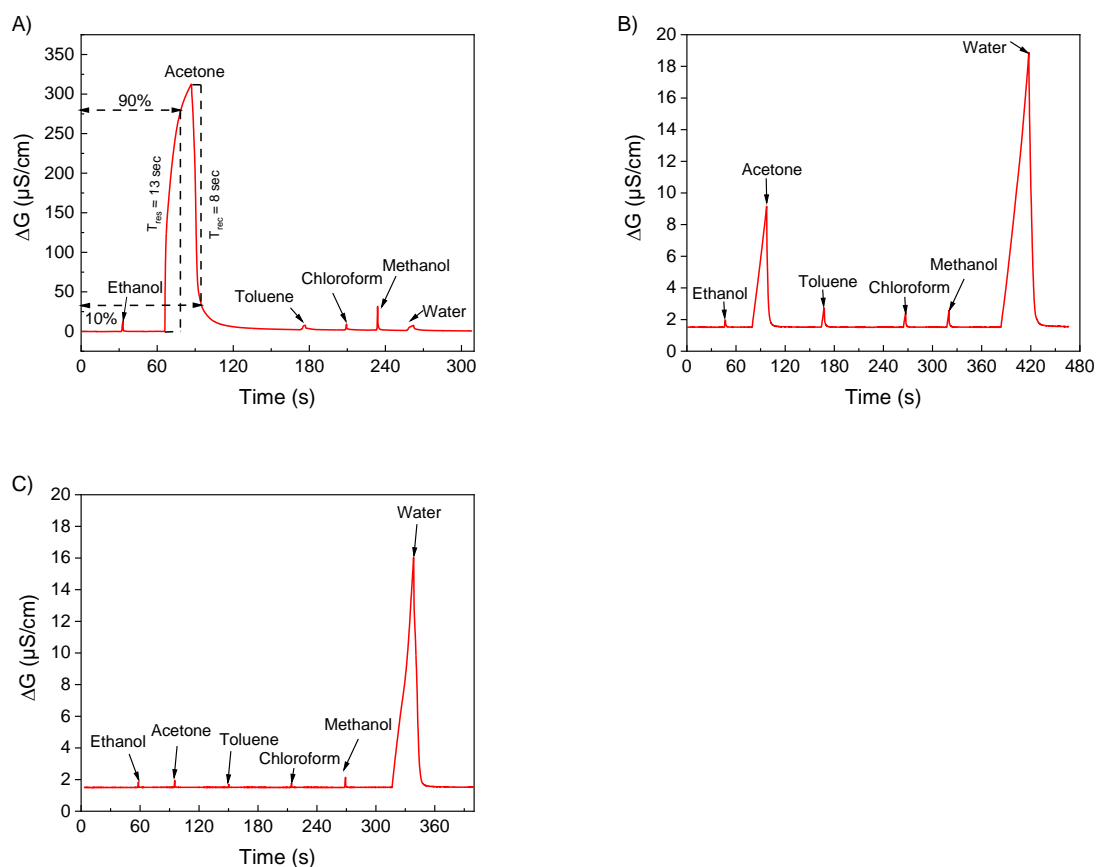


Fig. 8. Detection of gas-phase concentration for pure liquid phase of ethanol, acetone, toluene, chloroform, methanol, and water using differential output signal between the working A) PPy-PPyBF₄ sensor) B) PPy-PPyPF₆ C) PPy-PPyTFSI and the reference (PPy sensor).

We then measured the response of the PPy-PPyBF₄ sensor towards different acetone/water solutions at various concentrations (Fig. 9A). The sensor's conductance increases with an increase in the concentration of acetone in the liquid phase (from 2.8 v/v to 56.6 v/v%). The calibration curve of our developed sensor is presented in Fig. 9B. An excellent linearity ($R^2 = 0.9978$) and a sensitivity of $5.83 \mu\text{S}\cdot\text{cm}^{-1} (\text{v/v}\%)^{-1}$ are obtained. The detection limit of the developed acetone sensor is 0.76 v/v % (7600 ppm) in the gas phase. The relative standard deviation for the same sensor (five determinations) is 6% for lower concentrations and 2% for

higher concentrations. The response time (t_{Res}) of the microconductometric PPy-PPyBF₄ acetone sensor varies from 0.67 to 13 s from lower concentrations to higher concentrations (Fig. 6) whereas the time to recover (t_{Rec}) to the baseline immediately after removal from the headspace varies from 0.5 to 8 s. The measured sensitivity is $2.74 \mu\text{S}\cdot\text{cm}^{-1} (\text{v}/\text{v}\%)^{-1}$ for ethanol vapor and $1.27 \mu\text{S}\cdot\text{cm}^{-1} (\text{v}/\text{v}\%)^{-1}$ for methanol vapor. This makes our PPy-PPyBF₄ sensor twice more sensitive towards acetone than to ethanol and more than four times more sensitive towards acetone than to methanol.

The reproducibility was studied using 5 different acetone sensors. The sensor keeps its sensitivity of detection for six months, when kept at room temperature between the measurements.

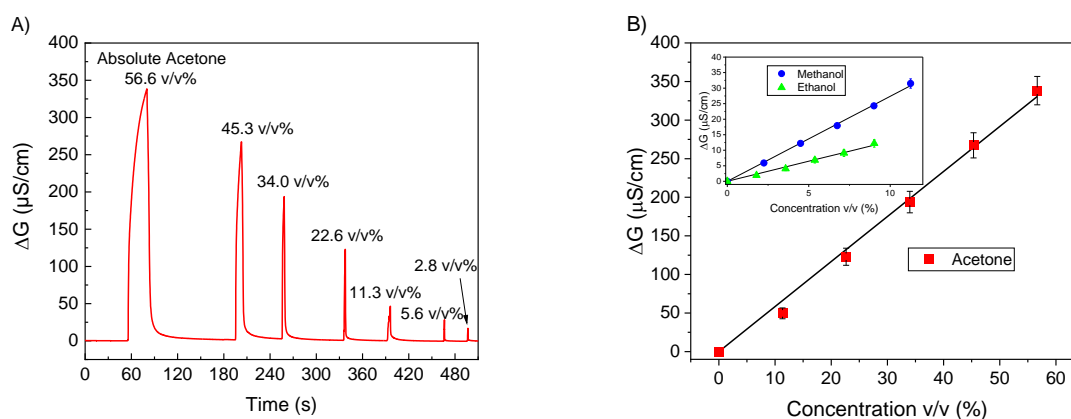


Fig. 9. A) Detection of gas-phase concentration for different Acetone/water solutions with PPy-PPyBF₄ sensor, using a lock-in amplifier. B) Calibration curve of the gas-phase concentrations of acetone, ethanol, and methanol.

3.6. Application of the acetone sensor: detection of acetone in the headspace of a nail varnish remover sample

The acetone content in the gas phase of a nail varnish remover was determined with our PPy-PPyBF₄ sensor (Fig. 10). For this, we initially measured the conductivity in the gas phase of absolute acetone and of an 80% acetone/water mixture. The conductivity found in the nail varnish remover sample gas phase was $260.8 \mu\text{S}/\text{cm}$. According to the calibration curve in Fig.9, this value corresponds to $44.69 \pm 0.75 \text{ v}/\text{v}\%$ in gas phase. The determined concentration of a nail varnish remover is $10.68 \pm 0.18 \text{ M}$ corresponding to $78.9 \pm 1.4 \%$ which is in good agreement with the value given by the producer, 75%.

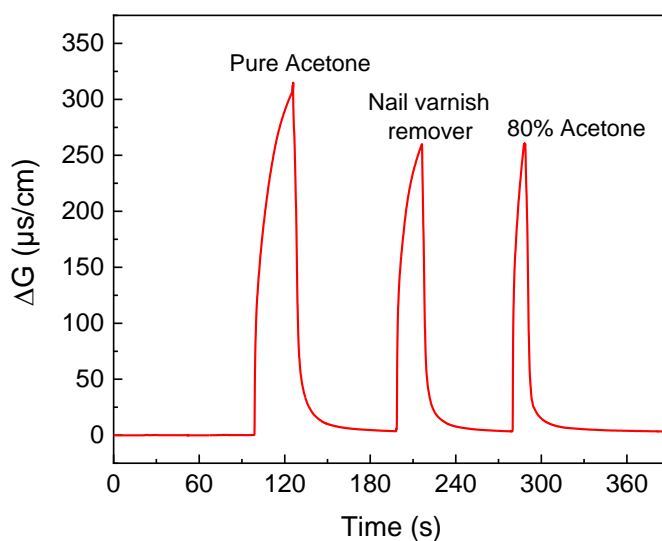


Fig. 10. Detection of gas-phase concentrations for different acetone/water solutions and commercial nail varnish remover, with PPy-PPyBF₄ sensor.

4. CONCLUSION

Conductimetric sensors were prepared by electropolymerization of pyrrole-functionalized imidazolium ionic liquids (ILs) monomer bearing different anions on gold-coated microconductimetric chips. An efficient adhesion of the pyrrole-functionalized IL was obtained thanks to the pre-deposition of pyrrole. The efficiency of the functionalization was assessed by IR spectroscopy, XPS analyses, and water contact angles measurements. The morphology of the resulting films depends on the anions used. PF₆⁻ and TFSI anions led to the formation of polypyrrole aggregates of about 1 μm of diameter while with BF₄⁻, aggregates of 10 μm of diameter were obtained. In line with this different morphological features, electrochemical impedance spectroscopy measurements have shown that the charge transfer resistance (R_{ct}) values are very close for PPy-PPyPF₆ and PPy-PPyTFSI samples, around 30 Ω while the PPy-PPyBF₄ sensor presents a higher R_{ct} value of 121 Ω. The analytical performances of the microsensors for the sensing of different solvents (ethanol, acetone, toluene, chloroform, methanol, and water) were tested in the gas phase at room temperature. Only the sensor bearing the BF₄⁻ anions responds to solvent vapor and this sensor is twice more sensitive towards acetone than to ethanol and more than four times more sensitive towards acetone than to methanol. The detection limit of the developed acetone sensor is 0.76 v/v % (7600 ppm) with a relative standard deviation ranging from 2 to 6% at

higher and lower acetone concentrations, respectively. The sensor presents good response and recovery times especially at low acetone concentration ($t_{Res}= 0.67s$ and $t_{Rec}= 0.5s$). The higher sensitivity for the sensor bearing BF_4^- anions over the other anions is due to less hydrogen bonding between the imidazolium cation and the anions that are thus more prone to interact with molecular solvent. The differences in hydrogen bonding also explain the higher sensitivity of the solvent towards acetone that is more polar. This sensor was further tested to determine the concentration of a nail varnish remover. The concentration of 78% found is in good agreement with the concentration of 75% furnished by the manufacturer.

To improve the sensor performance, we now plan to mix our films with gold nanoparticles.

Authors contribution

The manuscript was written through contributions of all authors. All authors have given approval to the final version of the manuscript.

Supporting Information. Experimental details, 1H , $^{13}C\{^1H\}$, ^{19}F NMR spectra, and Infra-Red spectra for all compounds, tables of equilibrium gas-phase concentrations (PDF). The following file is available free of charge.

Conflicts of interests

There are no conflicts to declare.

ACKNOWLEDGMENTS

The authors would like to thank Dr. Nicolas Rouge from the Plateforme Chimie UTINAM for recording SEM images. Thanks is due to ARCEN-Carnot platform (ICB) for XPS analysis (A. Krystianiak).

Funding

This research was funded by the Regional Council of Bourgogne Franche-Comté through the Envergure Program MatElectroCap and the PIA-excellence ISITE-BFC (COMICS project “Chemistry of Molecular Interactions Catalysis and Sensors” FEDER).

REFERENCES

1. Weber, M.; Pompetzki, W.; Bonmann, R.; Weber, M., Acetone. In *Ullmann's Encyclopedia of Industrial Chemistry*, pp 1-19.
2. Remler, R. F., The Solvent Properties of Acetone. *Ind. Eng. Chem.* **1923**, *15* (7), 717-720.
3. Joshi, D. R.; Adhikari, N., An Overview on Common Organic Solvents and Their Toxicity. *J. Pharm. Res. Int.* **2019**, *28* (3), 1-18.
4. Verma, A.; Yadav, D.; Singh, A.; Gupta, M.; Thapa, K. B.; Yadav, B. C., Detection of acetone via exhaling human breath for regular monitoring of diabetes by low-cost sensing device based on perovskite BaSnO₃ nanorods. *Sens. Actuators, B* **2022**, *361*, 131708.
5. Gao, X.; Zhang, T., An overview: Facet-dependent metal oxide semiconductor gas sensors. *Sens. Actuators, B* **2018**, *277*, 604-633.
6. Patil, S. J.; Patil, A. V.; Dighavkar, C. G.; Thakare, K. S.; Borase, R. Y.; Nandre, S. J.; Deshpande, N. G.; Ahire, R. R., Semiconductor metal oxide compounds based gas sensors: A literature review. *Front. Mater. Sci.* **2015**, *9* (1), 14-37.
7. Forleo, A.; Francioso, L.; Capone, S.; Siciliano, P.; Lommens, P.; Hens, Z., Synthesis and gas sensing properties of ZnO quantum dots. *Sens. Actuators, B* **2010**, *146* (1), 111-115.
8. Li, X.; Chang, Y.; Long, Y., Influence of Sn doping on ZnO sensing properties for ethanol and acetone. *Mater. Sci. Eng., C* **2012**, *32* (4), 817-821.
9. Cao, S.; Sui, N.; Zhang, P.; Zhou, T.; Tu, J.; Zhang, T., TiO₂ nanostructures with different crystal phases for sensitive acetone gas sensors. *J. Colloid Interface Sci.* **2022**, *607*, 357-366.
10. Li, W. Q.; Ma, S. Y.; Luo, J.; Mao, Y. Z.; Cheng, L.; Gengzang, D. J.; Xu, X. L.; Yan, S. H., Synthesis of hollow SnO₂ nanobelts and their application in acetone sensor. *Mater. Lett.* **2014**, *132*, 338-341.
11. Shi, J.; Hu, G.; Sun, Y.; Geng, M.; Wu, J.; Liu, Y.; Ge, M.; Tao, J.; Cao, M.; Dai, N., WO₃ nanocrystals: Synthesis and application in highly sensitive detection of acetone. *Sens. Actuators, B* **2011**, *156* (2), 820-824.

12. Bartlett, P. N.; Ling-Chung, S. K., Conducting polymer gas sensors Part III: Results for four different polymers and five different vapours. *Sensor Actuators* **1989**, *20* (3), 287-292.
13. Husain, A.; Shariq, M. U., Polypyrrole nanocomposites as promising gas/vapour sensing materials: Past, present and future prospects. *Sens. Actuators, A* **2023**, *359*, 114504.
14. Do, J.-S.; Wang, S.-H., On the sensitivity of conductimetric acetone gas sensor based on polypyrrole and polyaniline conducting polymers. *Sens. Actuators, B* **2013**, *185*, 39-46.
15. Ruangchuay, L.; Sirivat, A.; Schwank, J., Electrical conductivity response of polypyrrole to acetone vapor: effect of dopant anions and interaction mechanisms. *Synth. Met.* **2004**, *140* (1), 15-21.
16. Milella, E.; Musio, F.; Alba, M. B., Polypyrrole LB multilayer sensitive films for odorants. *Thin Solid Films* **1996**, *284-285*, 908-910.
17. Jun, H.-K.; Hoh, Y.-S.; Lee, B.-S.; Lee, S.-T.; Lim, J.-O.; Lee, D.-D.; Huh, J.-S., Electrical properties of polypyrrole gas sensors fabricated under various pretreatment conditions. *Sens. Actuators, B* **2003**, *96* (3), 576-581.
18. Nigorikawa, K.; Kunugi, Y.; Harima, Y.; Yamashita, K., A selective gas sensor using a polypyrrole thin film as a sensitive matrix on a piezoelectric crystal. *J. Electroanal. Chem.* **1995**, *396* (1), 563-567.
19. Yu, J.-B.; Byun, H.-G.; So, M.-S.; Huh, J.-S., Analysis of diabetic patient's breath with conducting polymer sensor array. *Sens. Actuators, B* **2005**, *108* (1), 305-308.
20. Adhikari, A.; Kar, P.; Rana, D.; De, S.; Nath, J.; Dutta, K.; Chattopadhyay, D., Synthesis of sodium cholate mediated rod-like polypyrrole-silver nanocomposite for selective sensing of acetone vapor. *Nano-Struct. Nano-Objects* **2020**, *21*, 100419.
21. Šetka, M.; Bahos, F. A.; Chmela, O.; Matatagui, D.; Gràcia, I.; Drbohlavová, J.; Vallejos, S., Cadmium telluride/polypyrrole nanocomposite based Love wave sensors highly sensitive to acetone at room temperature. *Sens. Actuators, B* **2020**, *321*, 128573.
22. Jamalabadi, H.; Alizadeh, N., Enhanced Low-Temperature Response of PPy-WO₃ Hybrid Nanocomposite Based Gas Sensor Deposited by Electrospinning Method For Selective and Sensitive Acetone Detection. *IEEE Sensors Journal* **2017**, *17* (8), 2322-2328.
23. Adhikari, M.; Das, S.; Chattopadhyay, D.; Saha, D.; Pal, M., Room-Temperature High-Performance Trace Level Acetone Sensor Based on Polypyrrole Nanotubes. *ChemNanoMat* *9* (n/a), e202300191.
24. Lei, Z.; Dai, C.; Chen, B., Gas Solubility in Ionic Liquids. *Chem. Rev.* **2014**, *114* (2), 1289-1326.

25. Rehman, A.; Zeng, X., Methods and approaches of utilizing ionic liquids as gas sensing materials. *RSC Adv.* **2015**, *5* (72), 58371-58392.
26. Gębicki, J.; Kloskowski, A.; Chrzanowski, W.; Stepnowski, P.; Namiesnik, J., Application of Ionic Liquids in Amperometric Gas Sensors. *Crit. Rev. Anal. Chem.* **2016**, *46* (2), 122-138.
27. Liang, C.; Yuan, C.-Y.; Warmack, R. J.; Barnes, C. E.; Dai, S., Ionic Liquids: A New Class of Sensing Materials for Detection of Organic Vapors Based on the Use of a Quartz Crystal Microbalance. *Anal. Chem.* **2002**, *74* (9), 2172-2176.
28. Tao, W.; Lin, P.; Liu, S.; Xie, Q.; Ke, S.; Zeng, X., 1-Butyl-3-Methylimidazolium Tetrafluoroborate Film as a Highly Selective Sensing Material for Non-Invasive Detection of Acetone Using a Quartz Crystal Microbalance. *Sensors* **2017**, *17* (1), 194.
29. Nishan, U.; Bashir, F.; Muhammad, N.; Khan, N.; Rahim, A.; Shah, M.; Nazir, R.; Sayed, M., Ionic liquid as a moderator for improved sensing properties of TiO₂ nanostructures for the detection of acetone biomarker in diabetes mellitus. *J. Mol. Liq.* **2019**, *294*, 111681.
30. Mecerreyes, D., Polymeric ionic liquids: Broadening the properties and applications of polyelectrolytes. *Prog. Polym. Sci.* **2011**, *36* (12), 1629-1648.
31. Guterman, R.; Ambroggi, M.; Yuan, J., Harnessing Poly(ionic liquid)s for Sensing Applications. *Macromol. Rapid Commun.* **2016**, *37* (14), 1106-1115.
32. Zhao, Q.; Heyda, J.; Dzubiella, J.; Täuber, K.; Dunlop, J. W. C.; Yuan, J., Sensing Solvents with Ultrasensitive Porous Poly(ionic liquid) Actuators. *Adv. Mater.* **2015**, *27* (18), 2913-2917.
33. Zhao, Q.; Dunlop, J. W. C.; Qiu, X.; Huang, F.; Zhang, Z.; Heyda, J.; Dzubiella, J.; Antonietti, M.; Yuan, J., An instant multi-responsive porous polymer actuator driven by solvent molecule sorption. *Nat. Commun.* **2014**, *5* (1), 4293.
34. Tung, T. T.; Castro, M.; Kim, T. Y.; Suh, K. S.; Feller, J.-F., High stability silver nanoparticles–graphene/poly(ionic liquid)-based chemoresistive sensors for volatile organic compounds' detection. *Anal. Bioanal. Chem.* **2014**, *406* (16), 3995-4004.
35. Halima, H. B.; Zwingelstein, T.; Humblot, V.; Lakard, B.; Viau, L., Electropolymerization of Pyrrole-Tailed Imidazolium Ionic Liquid for the Elaboration of Antibacterial Surfaces. *ACS Appl. Mater. Inter.* **2023**, *15* (28), 33382-33396.
36. Zhang, W.; Li, Y.; Lin, C.; An, Q.; Tao, C.; Gao, Y.; Li, G., Electrochemical polymerization of imidazolium-ionic liquids bearing a pyrrole moiety. *J. Polym. Sci., Part A: Polym. Chem.* **2008**, *46* (12), 4151-4161.

37. Johanson, U.; Marandi, M.; Tamm, T.; Tamm, J., Comparative study of the behavior of anions in polypyrrole films. *Electrochim. Acta* **2005**, *50* (7), 1523-1528.
38. Sander, R., *Compilation of Henry's Law Constants for Inorganic and Organic Species of Potential Importance in Environmental Chemistry*. Max-Planck Institute of Chemistry, Air Chemistry Department: 1999.
39. Snider, J. R.; Dawson, G. A., Tropospheric light alcohols, carbonyls, and acetonitrile: Concentrations in the southwestern United States and Henry's Law data. *Journal of Geophysical Research: Atmospheres* **1985**, *90* (D2), 3797-3805.
40. Fairley, N.; Fernandez, V.; Richard-Plouet, M.; Guillot-Deudon, C.; Walton, J.; Smith, E.; Flahaut, D.; Greiner, M.; Biesinger, M.; Tougaard, S.; Morgan, D.; Baltrusaitis, J., Systematic and collaborative approach to problem solving using X-ray photoelectron spectroscopy. *Appl. Surf. Sci. Adv.* **2021**, *5*, 100112.
41. Liang, X.; Wen, Z.; Liu, Y.; Wang, X.; Zhang, H.; Huang, M. W. L., Preparation and characterization of sulfur-polypyrrole composites with controlled morphology as high capacity cathode for lithium batteries. *Solid State Ionics* **2011**, *192* (1), 347-350.
42. Viau, L.; Hihn, J. Y.; Lakard, S.; Moutarlier, V.; Flaud, V.; Lakard, B., Full characterization of polypyrrole thin films electrosynthesized in room temperature ionic liquids, water or acetonitrile. *Electrochim. Acta* **2014**, *137*, 298-310.
43. Yamada, T.; Tominari, Y.; Tanaka, S.; Mizuno, M., Infrared Spectroscopy of Ionic Liquids Consisting of Imidazolium Cations with Different Alkyl Chain Lengths and Various Halogen or Molecular Anions with and without a Small Amount of Water. *J. Phys. Chem. B* **2017**, *121* (14), 3121-3129.
44. Yamada, T.; Mizuno, M., Infrared and Terahertz Spectroscopic Investigation of Imidazolium, Pyridinium, and Tetraalkylammonium Tetrafluoroborate Ionic Liquids. *ACS Omega* **2022**, *7* (34), 29804-29812.
45. Talaty, E. R.; Raja, S.; Storhaug, V. J.; Dölle, A.; Carper, W. R., Raman and Infrared Spectra and ab Initio Calculations of C2-4MIM Imidazolium Hexafluorophosphate Ionic Liquids. *J. Phys. Chem. B* **2004**, *108* (35), 13177-13184.
46. Rey, I.; Johansson, P.; Lindgren, J.; Lassègues, J. C.; Grondin, J.; Servant, L., Spectroscopic and Theoretical Study of $(\text{CF}_3\text{SO}_2)_2\text{N}^-$ (TFSI) and $(\text{CF}_3\text{SO}_2)_2\text{NH}$ (HTFSI). *J. Phys. Chem. A* **1998**, *102* (19), 3249-3258.
47. Hashimoto, H.; Ohno, A.; Nakajima, K.; Suzuki, M.; Tsuji, H.; Kimura, K., Surface characterization of imidazolium ionic liquids by high-resolution Rutherford backscattering spectroscopy and X-ray photoelectron spectroscopy. *Surf. Sci.* **2010**, *604* (3), 464-469.

48. Lovelock, K. R. J.; Villar-Garcia, I. J.; Maier, F.; Steinrück, H.-P.; Licence, P., Photoelectron Spectroscopy of Ionic Liquid-Based Interfaces. *Chem. Rev.* **2010**, *110* (9), 5158-5190.
49. Seo, S.; Park, J.; Kang, Y.-C., Chemical Analysis of Ionic Liquids Using Photoelectron Spectroscopy. *Bull. Korean Chem. Soc.* **2016**, *37* (3), 355-360.
50. Kwon, O. S.; Hong, J.-Y.; Park, S. J.; Jang, Y.; Jang, J., Resistive Gas Sensors Based on Precisely Size-Controlled Polypyrrole Nanoparticles: Effects of Particle Size and Deposition Method. *J. Phys. Chem. C* **2010**, *114* (44), 18874-18879.
51. Trenzado, J. L.; Gutiérrez, A.; Alcalde, R.; Atilhan, M.; Aparicio, S., Insights on [BMIM][BF₄] and [BMIM][PF₆] ionic liquids and their binary mixtures with acetone and acetonitrile. *J. Mol. Liq.* **2019**, *294*, 111632.
52. Gozzo, F. C.; Santos, L. S.; Augusti, R.; Consorti, C. S.; Dupont, J.; Eberlin, M. N., Gaseous Supramolecules of Imidazolium Ionic Liquids: “Magic” Numbers and Intrinsic Strengths of Hydrogen Bonds. *Chem. Eur. J.* **2004**, *10* (23), 6187-6193.
53. Wang, P.; Zhang, X.; Gao, S.; Cheng, X.; Sui, L.; Xu, Y.; Zhao, X.; Zhao, H.; Huo, L., Superior acetone sensor based on single-crystalline α -Fe₂O₃ mesoporous nanospheres via [C₁₂mim][BF₄]-assistant synthesis. *Sens. Actuators, B* **2017**, *241*, 967-977.
54. Zhai, C.; Wang, J.; Zhao, Y.; Tang, J., A NMR Relaxation Study for the Interactions of some 1-alkyl-3-methylimidazolium Ionic Liquids with Acetone. *Z. Phys. Chem.* **2009**, *223* (8), 839-847.

For Table of Contents Only

